ELSEVIER

Journal of Power Sources 89 (2000) 15–28

JOURNAL OF POWER SOURCES

www.elsevier.com/locate/jpowsour

Effect of electrode parameters on charge performance of a lead–acid cell

Sung Chul Kim, Won Hi Hong *

Department of Chemical Engineering, Korea Advanced Institute of Science and Technology, 373-1 Kusung-dong, Yusung-gu, Taejeon 305-701, South Korea

Received 27 September 1999; accepted 10 December 1999

Abstract

The charge characteristics of a lead–acid cell are observed by using a numerical simulation. The effect of various parameters, such as the concentration exponent of charge reaction, morphology parameter and limiting current density, on the cell voltage during charge has been investigated by including the dissolution–precipitation mechanism of the negative electrode. As the charging current density is increased, the concentration gradient is increased due to the high resistance of the electrolyte migration, especially at the interface between the positive electrode and the reservoir.

Keywords: Lead–acid cell; Charge; Electrode kinetics; Mathematical modeling

1. Introduction

One of the important factors needed to use the batteries for electric vehicles is the possibility of fast charging. For fast recharging, high currents are required. This method, however, is expected to cause excessive heating of the batteries. Overheating severely reduces cycle-life. Therefore, a method is required to charge the batteries quickly without damage.

Maja et al. [1] examined the effect of different parameters, such as plate dimensions, amount of acid, porosity of active material and modality of charging, on the charge performance. Valeriote and Jochim [2] studied the key components to reduce temperature increase for charging the battery. They found that the temperature rise was determined not only by the amount of heat produced by the charge process but also by the rate of heat dissipation and the heat capacity of the battery. The effects of charging current, depth-of-discharge and battery design were observed in the charge process. Chang et al. [3] discussed fast-charging effects on hybrid lead–acid batteries which contained antimonial positive grids and non-antimonial negative grids. They used the constant resistance-free voltage which compensated for the ohmic voltage drop to reduce the internal resistance of the battery.

Gu et al. [4] compared the voltage penalty and time to the voltage cut-off at moderate and low temperature, respectively. Gu et al. [5] developed the model not only to account for coupled processes of electrochemical kinetics and mass transport occurring in a battery cell, but also to consider free convection resulting from density variations due to acid stratification. These two investigations only considered the charge transfer in the electrode kinetics of the negative electrode during charge and did not take into account the solid-state reaction.

Ekdunge et al. [6] showed that the cathodic polarization curves at different states of charge exhibited limiting-current phenomena due to rate-determining dissolution of lead sulfate or/and diffusion of lead ions.

In this study, we have incorporated the solid-state reaction, that is, the dissolution of lead sulfate and the diffusion of lead ions, and have developed a mathematical model to predict accurately the effect of various electrode parameters on the charge performance of a lead–acid cell.

2. Mathematical model

2.1. Governing equations

The approach presented here was based on a macroscopic model [4,7] and a mathematical model [8,9] which describe the discharge performance of a lead–acid cell.

* Corresponding author.

0378-7753/00/$ - see front matter
PII: S0378-7753(00)00377-3

The assumptions made in the development of the model are follows.

(i) The lead–acid cell consists of a lead dioxide electrode (PbO_2), an electrolyte reservoir, a porous separator, and a lead electrode (Pb).
(ii) Each electrode is a porous and electronically conductive matrix with pores occupied by sulfuric acid solution.
(iii) The model is one-dimensional in the direction perpendicular to the plane of the electrodes.
(iv) Porous electrodes are assumed to be macro-homogeneous.
(v) The cell can be considered to be isothermal during its operation.

During charge, the electrode reactions in a lead–acid cell are expressed as follows:

$$PbSO_4(s) + 2H_2O \rightarrow PbO_2(s) + HSO_4^- + 3H^+ + 2e^- \quad (I)$$

for the positive electrode, and

$$PbSO_4(s) + 2e^- + H^+ \rightarrow Pb(s) + HSO_4^- \quad (II)$$

for the negative electrode. Lead sulfate is converted to lead dioxide (positive electrode) and lead (negative electrode) during charge.

The kinetic behaviour of a lead electrode in a lead–acid cell is influenced by local activity, overpotential, electrolyte concentration, and current density distribution [6]. The reaction kinetics of the negative electrode assume that the charge reaction consists of two or more elementary reactions: dissolution of lead sulfate, diffusion of lead ions to an active lead surface, and electrochemical reactions. The transfer current, which the solid-state reaction is included in, is written as follows [8,9]:

$$j = ai_{o\,4,\mathrm{ref}}\left(1 - \frac{Q}{Q_{\max}}\right) \times \left(\frac{c}{c_{\mathrm{ref}}}\right)^{\gamma 4} \frac{1 - \exp\left[(\alpha_{a4} + \alpha_{c4})\frac{F\eta}{RT}\right]}{\frac{ai_{o4,\mathrm{ref}}}{j_{\lim}} - \exp\left[\alpha_{c4}\frac{F\eta}{RT}\right]} \quad (1)$$

where the limiting current density $j_{\lim}$ affects significantly the polarization curves and is determined from the dissolution rate of lead sulfate, the diffusion rate of lead ions, and the precipitation rate of lead crystals.

The total current density i is the sum of the current density in the solid phase i_1 and the current density in the conducting liquid phase i_2, i.e.,

$$i = i_1 + i_2. \quad (2)$$

The current density in the solid phase, i_1, follows Ohm's law. The current density in the electrolytic solution, i_2, is proportional not only to the concentration gradient but also to the electric potential gradient.

The material balance for the acid concentration in the liquid phase is given by convection, diffusion and migration of mobile ionic species. The volume-average velocity v^* is used as the reference velocity [10]. The effective diffusivity D^* is given by the diffusion coefficient of the electrolyte, porosity, and tortuosity [11]. The porosity of the electrode during charge is changed by the electrode reaction and is proportioned to the transfer current.

The overall electrode reaction-rate, j, in the positive electrode is represented by the Butler–Volmer equation. The overpotential η at this electrode is defined as:

$$\eta = \phi_1 - \phi_2 - U_{PbO_2} \quad (3)$$

where ϕ_1 is the potential of the solid phase and ϕ_2 is the potential of the liquid phase.U_{PbO_2} denotes equilibrium potential evaluated at a reference concentration c_{ref}.

The electroactive surface area, a, can be related to the state-of-charge. Note that the charging reaction should stop when lead sulfate formed on the previous step is completely converted [4], i.e.,

$$a\left(1 - \frac{Q}{Q_{\max}}\right) = a_{\max}\left(\frac{Q}{Q_{\max}}\right)^{s} \times \left(1 - \frac{Q}{Q_{\max}}\right) \quad (4)$$

where $a_{\max}$ denotes the maximum active surface area of the electrode; Q is the charge per unit volume of the electrode; $Q_{\max}$ is the maximum charge that can be extracted from the electrode.

The overall reaction-rate at the negative electrode is given by Eq. (1), which takes account of the solid-state reactions. The overpotential at this electrode is defined as:

$$\eta = \phi_1 - \phi_2. \quad (5)$$

The governing equations to develop the mathematical model are shown in Table 1 [8,9].

2.2. Initial and boundary conditions

The initial values for electrolyte concentration and porosity are as follows.

$$c = c_{\mathrm{ref}} \quad (6)$$

$$\varepsilon = \varepsilon_{PbO_2,\mathrm{ini}} \quad (7)$$

$$\varepsilon = \varepsilon_{Pb,\mathrm{ini}} \quad (8)$$

where Eqs. (7) and (8) relate to the positive and negative electrode, respectively. The initial potential distribution can be calculated from the equation for the electrode kinetic reaction.

The symmetry conditions, at the centres of the positive and negative electrode, are used to define the electrolyte concentration, porosity change, and the voltage of the solid phase. Because there is no electrolyte at these boundaries,

Table 1
Governing equations for each region

	Positive electrode	Reservoir	Separator	Negative electrode
Porosity variation	$(\partial\varepsilon/\partial t)=[1/(2F)]a_1 j$	$\varepsilon=1$	$\varepsilon=\varepsilon_{sep}$	$(\partial\varepsilon/\partial t)=[1/(2F)]a_1 j$
Ohm's law in solid	$i_1=\sigma^*\nabla\phi_1$	$i_1=0$	$i_1=0$	$i_1=\sigma^*\nabla\phi_1$
Ohm's law in liquid	$i_2=-\kappa^*\nabla\phi_2-\kappa^{**}\nabla(\ln c)$	$i_2=-\kappa^*\nabla\phi_2-\kappa^{**}(\ln c)$	$i_2=-\kappa^*\nabla\phi_2-\kappa^{**}\nabla(\ln c)$	$i_2=-\kappa^*\nabla\phi_2-\kappa^{**}\nabla(\ln c)$
Mass balance of electrolyte	$[\partial(\varepsilon c)/\partial t]+v^*\cdot\nabla c$ $=\nabla\cdot(D^*\nabla c)+[(a_2 j)/(2F)]$	$[\partial(\varepsilon c)/\partial t]+v^*\cdot\nabla c$ $=\nabla\cdot(D^*\nabla c)+[(a_2 j)/(2F)]$	$[\partial(\varepsilon c)/\partial t]+v^*\cdot\nabla c$ $=\nabla\cdot(D^*\nabla c)+[(a_2 j)/(2F)]$	$[\partial(\varepsilon c)/\partial t]+v^*\cdot\nabla c$ $=\nabla\cdot(D^*\nabla c)+[(a_2 j)/(2F)]$
Electrode kinetics	$j=ai_{o1,ref}\left(1-\frac{Q}{Q_{max}}\right)\left(\frac{c}{c_{ref}}\right)^{\gamma 1}\times\left[\exp\left(\alpha_{a1}\frac{F\eta}{RT}\right)-\exp\left(\alpha_{c1}\frac{F\eta}{RT}\right)\right]$	$\phi_1=0$	$\phi_1=0$	$j=ai_{o4,ref}\left(1-\frac{Q}{Q_{max}}\right)\left(\frac{c}{c_{ref}}\right)^{\gamma 4}\times\frac{1-\exp\left[(\alpha_{a4}+\alpha_{c4})\frac{F\eta}{RT}\right]}{\frac{ai_{o4,ref}}{j_{lim}}-\exp\left[\alpha_{c4}\frac{F\eta}{RT}\right]}$

Table 2
Boundary conditions for each region

Centers of positive and negative electrode	Interface between positive electrode and reservoir	Interface between reservoir and separator	Interface between separator and negative electrode
$\nabla c=0$	$\varepsilon^*\nabla c\|_+=\nabla c\|_{res}$	$D\cdot\nabla c-cv^*\|_{res}=D^*\cdot\nabla c-cv^*\|_{sep}$	$\varepsilon^*\nabla c\|_{sep}=\varepsilon^*\nabla c\|_-$
$\nabla\varepsilon=0$	$\varepsilon^*\nabla\phi_2\|_+=\nabla\phi_2\|_{res}$	$\varepsilon=\varepsilon_{sep}$	$\varepsilon^*\nabla\phi_2\|_{sep}=\varepsilon^*\nabla\phi_2\|_-$
$\nabla\phi_2=0$	$(\partial\varepsilon/\partial t)=[1/(2F)]a_1 j$	$i_2=i$	$(\partial\varepsilon/\partial t)=[1/(2F)]a_1 j$
$i_2=0$	$i_2=i$	$\phi_1=0$	$i_2=i$
$\phi_1=0$ (POS)			
$j=ai_{o4,ref}\left(1-\frac{Q}{Q_{max}}\right)\left(\frac{c}{c_{ref}}\right)^{\gamma 4}\times\frac{1-\exp\left[(\alpha_{a4}+\alpha_{c4})\frac{F\eta}{RT}\right]}{\frac{ai_{o1,ref4}}{j_{lim}}-\exp\left[\alpha_{c4}\frac{F\eta}{RT}\right]}$ (NEG)	$\nabla\phi_1=0$	$\nabla\phi_2-\frac{RT}{F}(1-2t_+^o)\nabla(\ln c)\|_{res}$ $=\varepsilon^*\left[\nabla\phi_2-\frac{RT}{F}(1-2t_+^o)\nabla(\ln c)\right]\|_{sep}$	$\nabla\phi_1=0$

Table 3
Coefficients and effective properties used in model equations

	Positive electrode	Reservoir	Separator	Negative electrode
a_1	$(MW_{PbSO_4}/\rho_{PbSO_4}) - (MW_{PbO_2}/\rho_{PbO_2})$	–	–	$(MW_{Pb}/\rho_{Pb}) - (MW_{PbSO_4}/\rho_{PbSO_4})$
a_2	$3 - 2t_+^o$	0	0	$1 - 2t_+^o$
σ^*	$\sigma_{PbO_2}\varepsilon^{exm1}$	–	–	$\sigma_{Pb}\varepsilon^{exm4}$
κ^*	$\kappa\varepsilon^{ex1}$	κ	$\kappa\cdot\ \varepsilon_{sep}^{ex3}$	$\kappa\varepsilon^{ex4}$
κ^{**}	$[(RT)/F]\kappa\varepsilon^{ex1}(2t_+^o - 1)$	$[(RT)/F]\kappa(2t_+^o - 1)$	$[(RT)/F]\kappa\cdot\ \varepsilon_{sep}^{ex3}(2t_+^o - 1)$	$[(RT)/F]\kappa\varepsilon^{ex4}(2t_+^o - 1)$
D^*	$D\varepsilon^{ex1}$	D	$D\varepsilon_{sep}^{ex3}$	$D\varepsilon^{ex4}$

the current density of the liquid phase is zero. At the centre of the positive electrode, the potential on the surface of the current collector is taken to be zero. The electrode kinetic equation is used to calculate the potential at the negative electrode.

Both the flux of the electrolyte and the current density in the liquid phase are continuous at the positive electrode solidus reservoir, reservoir solidus separator, and separator solidus negative electrode interfaces. From the assumption of electroneutrality, the charge is conserved at these regions. The variation of the porosity, at the positive electrode solidus reservoir and separator solidus negative electrode interfaces, is proportional to the rate of charge reaction. All the current flows through the liquid phase, because there is no solid electrode at the interface between the reservoir and the separator. The boundary conditions to solve the governing equations are shown in Table 2 and the coefficients used in the development of the model are presented in Table 3.

Table 4
Parameters used in calculations [8]

Parameter	Value
Positive electrode	
Half thickness of plate	0.0875 cm
Maximum charge state	2620 C cm^{-3}
Reaction parameter $(a_{max1}i_{o1,ref})$	0.073 A cm^{-3}
α_{a1}	1.15
α_{c1}	0.85
γ_1	0.01
ζ_1	1.0
Lead dioxide conductivity	500 S cm^{-1}
ex1	1.5
exm1	0.5
Negative electrode	
Half thickness of plate	0.07 cm
Maximum charge state	3120 C cm^{-3}
Reaction parameter $(a_{max4}i_{o4,ref})$	0.11 A cm^{-3}
α_{a4}	1.55
α_{c4}	0.45
γ_4	0.01
ζ_4	1.0
Lead conductivity	4.8×10^4 S cm^{-1}
ex4	1.5
exm4	0.5
j_{lim}	-10^2 A cm^{-3}
Reservoir	
Thickness of reservoir	0.07 cm
Separator	
Thickness of separator	0.022 cm
Porosity	0.60
ex3	1.50
Electrolyte	
Acid concentration	4.9×10^{-3} mol cm^{-3}
Transference number	0.72
Partial molar volume of acid	45 cm^{-3} mol
Diffusion coefficient	$D = \exp[(2174.0/298.15) - (2174.0/T)]\times(1.75 + 260.0c)\times10^{-5}$
Conductivity	$\kappa = c\times\exp\{1.1104 + (199.475 - 16097.781c)c + [(3916.95 - 99406.0c - (721860/T))/T]\}$

2.3. Numerical procedure

The space derivatives are discretized by the method of finite differences and the time derivatives are formulated by means of the Crank–Nicolson method. The non-linear, multi-region problems are solved by the Newton–Raphson iterative method [12] and MBAND [13]. The material properties and the cell parameters used in the simulation are presented in Table 4.

3. Results and discussion

The effect of various parameters, such as the charge-reaction concentration exponent, morphology parameter and limiting current density on the charge performance is investigated by using the mathematical model. The parameter γ denotes the concentration dependence on the charge reaction, and ζ is the morphology parameter which is used to account for the way lead sulfate covers the electrode surface. The morphology parameter, ζ, has a large value if the lead sulfate is spread well over the electrode surface. The limiting current density, j_{lim}, denotes the solid-state reaction rate when the lead precipitates from lead sulfate in the negative electrode. For constant-current charge, the charging current density was changed and the cell performance was evaluated. The battery used in the simulation

was discharged with 1.7 mA cm^{-2} for 8 h at 25°C followed by a rest period for 1 h at the same temperature.

The effect of the concentration exponent of charge reaction, γ, on the cell voltage when the battery was charged at 10 mA cm^{-2} is shown in Fig. 1. The parameter, γ, which corresponds to the reaction-rate order in the chemical reaction, was incorporated to accommodate the electrolyte concentration dependence on the exchange current density. The effect of γ_1 in the positive electrode is simulated in Fig. 1(a). As γ_1 is increased, the concentration dependence on the electrode reaction-rate is increased and the voltage penalty becomes higher at the beginning of charge. After the charge process has progressed at some degree, it can be seen that the cell voltage profiles at the three values of γ_1 become similar. At the initial state-of-charge, the electrolyte concentration does not cause significant change of the reaction rate in the positive electrode. By contrast, the electrolyte concentration is an important parameter in the negative electrode, where lead sulfate reacts with hydrogen ions. The voltage penalty increases with increasing the dependence of the electrolyte concentration at the start-of-charge, as shown in Fig. 1(b). The slope of voltage increment becomes higher as γ_4 is decreased in the negative electrode.

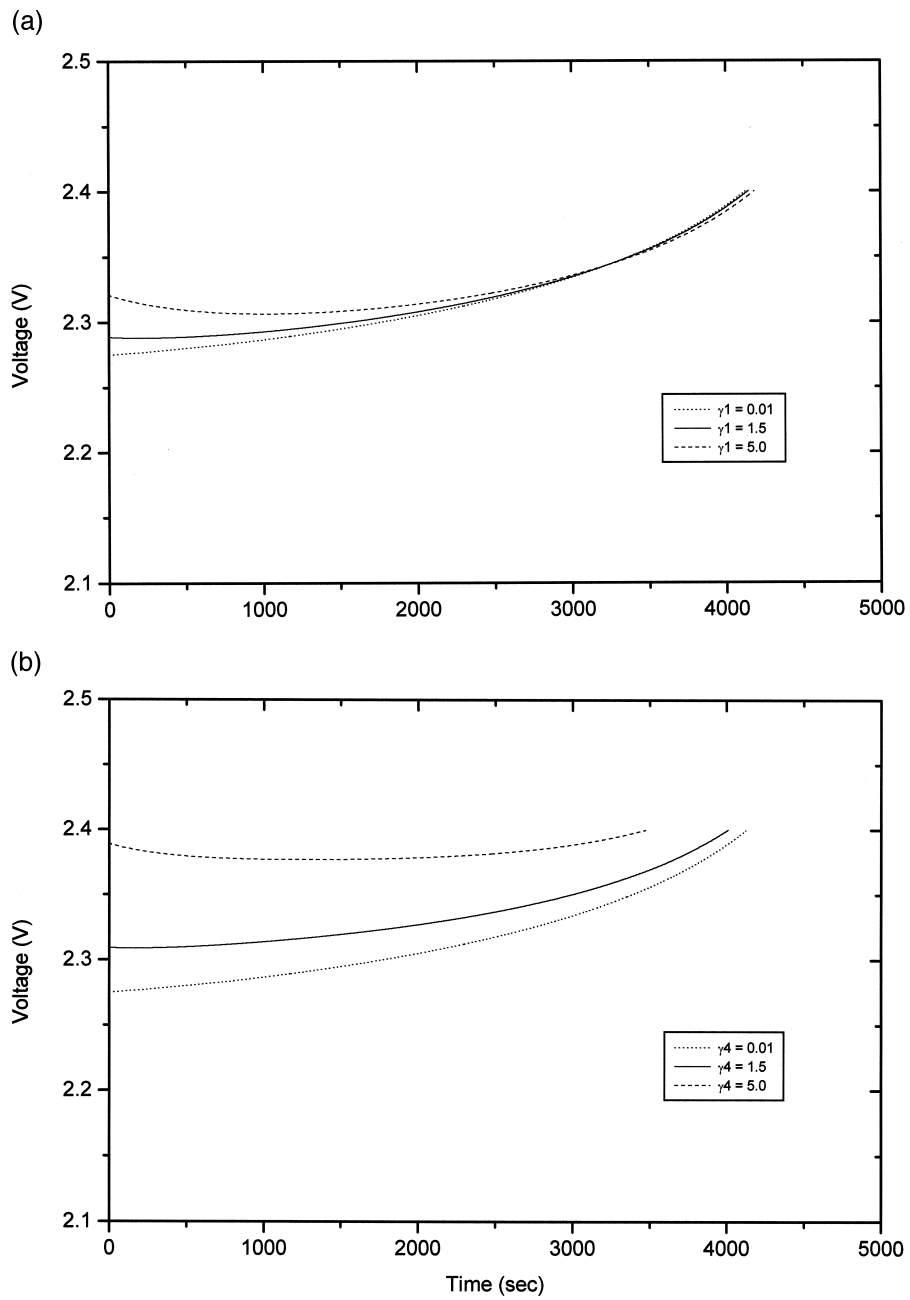

Fig. 1. Effect of charge-reaction concentration exponent for 10 mA cm^{-2} charge at 25°C: (a) positive electrode, (b) negative electrode.

The effect of the morphology parameter on the cell voltage is shown in Fig. 2. The slope of the voltage increment at the initial state increases with increasing value of ζ_1 in the positive electrode. This means that the electro-active area at the beginning of charge is low and, thereby, increases the internal resistance of the cell. Therefore, the morphology parameter of the positive electrode ζ_1 has a strong influence on the increment of the cell voltage at the beginning of charge.

The effect of the morphology parameter in the negative electrode on the cell voltage is analogous to that in the positive electrode. The higher value of ζ_4 will have a greater effect on the voltage increment at the initial state-of-charge. This is because nonconductor lead sulfate spreads uniformly over the surface of the negative electrode and the negative electrode of higher value of ζ_4 has lower electrical conductivity. When ζ_4 has a low value, the lead sulfate crystal grows in a needle-like shape on the surface of the lead electrode during discharge [14]. Consequently, there is no discernible difference in the electrical conductivity of lead electrode between the initial and the end of discharge. The increment of voltage is, therefore, much lower in the case of a high value of ζ_4 than in that of a low value.

The effect of the solid-state reaction in the lead electrode (i.e., the dissolution of lead sulfate, the diffusion of

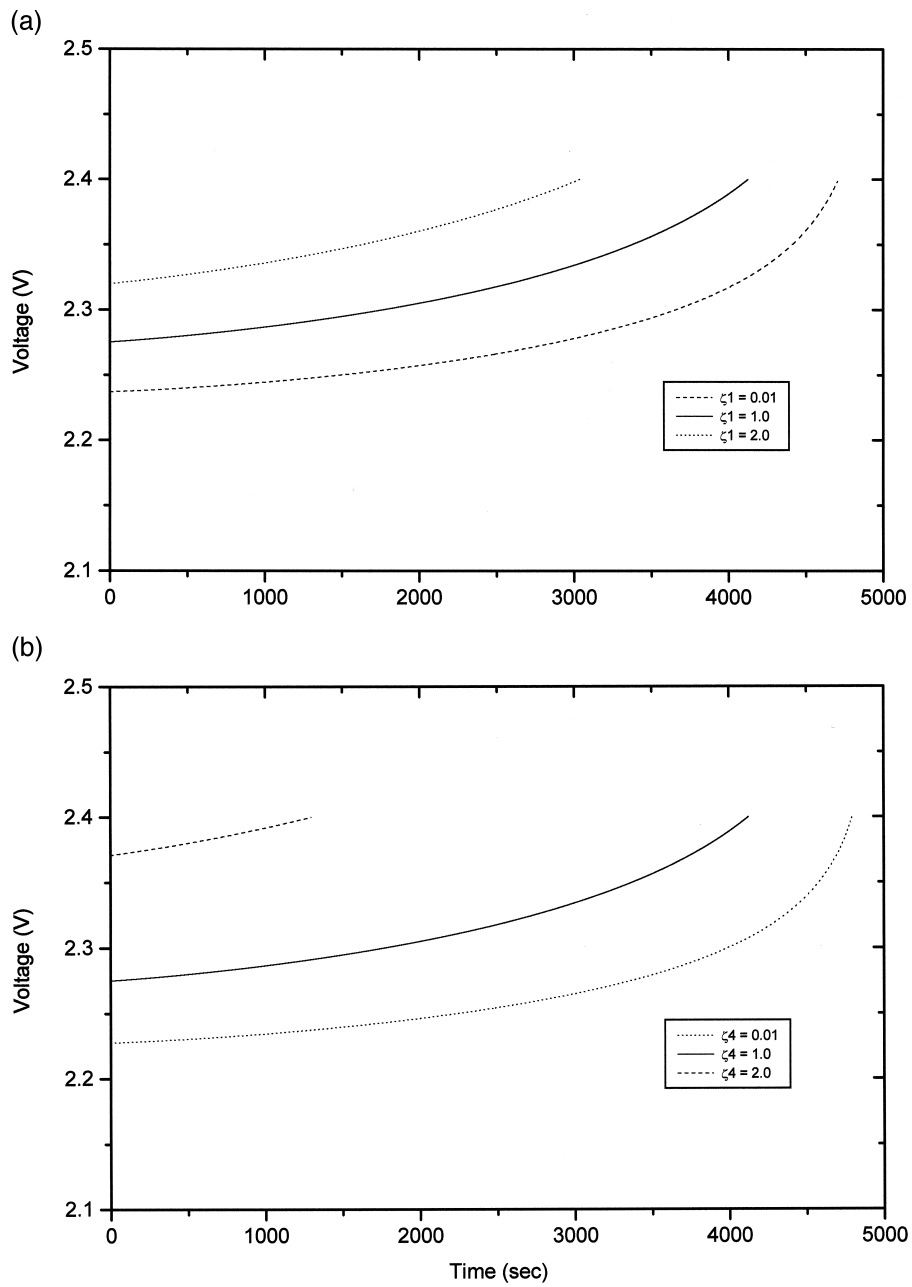

Fig. 2. Effect of morphology parameter for 10 mA cm^{-2} charge at 25°C: (a) positive electrode, (b) negative electrode.

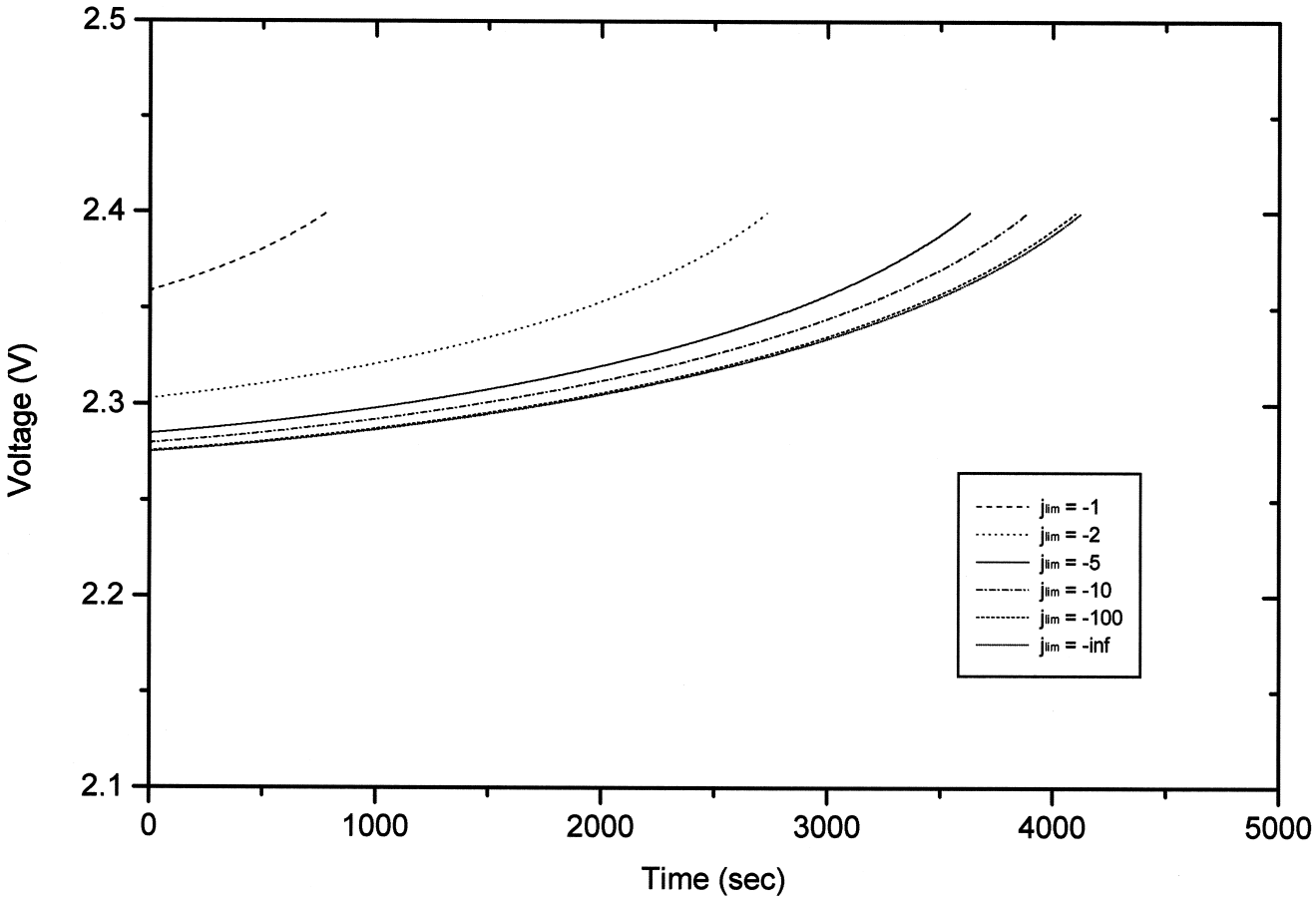

Fig. 3. Effect of limiting current density in negative electrode for 10 mA cm^{-2} charge at 25°C.

lead to the active surface, and the precipitation of lead crystal) on the charge performance is presented in Fig. 3. The limiting current density is determined by the limiting dissolution rate of lead sulfate or by the limiting diffusion rate of lead ions, or by a combination of both. For a lower absolute value of the limiting current density, the solid-reaction rate controls the overall reaction rate in the negative electrode during charge [6]. If the solid-state reaction rate is much higher than the charge-transfer reaction rate, the absolute value of j_{lim} becomes higher. This implies that the predicted voltage profile for the solid-state reaction at the negative electrode will have the same behaviour as in the case of including only the charge-transfer reaction. The cell voltage increases rapidly with decreasing $-j_{\text{lim}}$ due to the higher initial voltage during charge. Therefore, if the solid-state reaction rate in the negative electrode is low, the charge efficiency becomes lower due to the high internal resistance of the cell.

The distribution of the electrolyte concentration in the cell for various limiting current densities, under the same conditions as in Fig. 3, is given in Fig. 4. The predicted profile, the electrolyte concentration or a limiting current density, j_{lim}, of -1.0 A cm^{-3} is shown in Fig. 4(a). If the absolute value of the limiting current density is low, the rate of solid-state reaction controls that of the electrode reaction in the negative electrode. It is found that only 16% of the previous discharge has been restored. Although the concentration gradient in the negative electrode is not steeper, the polarization resistance becomes higher due to the slow rate of the solid-state reaction. In the electric field, the electrolyte concentration in the positive electrode is higher than that in the negative due to the migration resistance of the HSO_4^- ions [15]. The limiting current density is taken to be -5.0 A cm^{-3} in Fig. 4(b). Thus, the solid-state reaction rate is faster in Fig. 4(b) than in 4(a). At 100 s, for the electrolyte distribution there is no significant difference between cases (a) and (b). The charge returned is about 74%. When the limiting current density is set to -10.0 A cm^{-3}, as shown in Fig. 4(c), the behaviour of the electrolyte concentration is similar to Fig. 4(b) and about 79% has been returned. If the solid-state reaction rate is very fast, the rate-determining step in the electrode reaction becomes the charge-transfer rate, as represented in Fig. 4(d). It is shown, in this case, that the charge restored is about 84%. From the results given in Fig. 4(a)–(d), it is concluded that the limiting current density affects significantly the initial voltage rise, while it has only a very little influence on the concentration gradient in the cell, when the charging current density is constant.

The cell voltage is demonstrated in Fig. 5 for charging current densities. When the charging current densities are set to 1, 5, 10 and 20 mA cm^{-2}, respectively, the times to

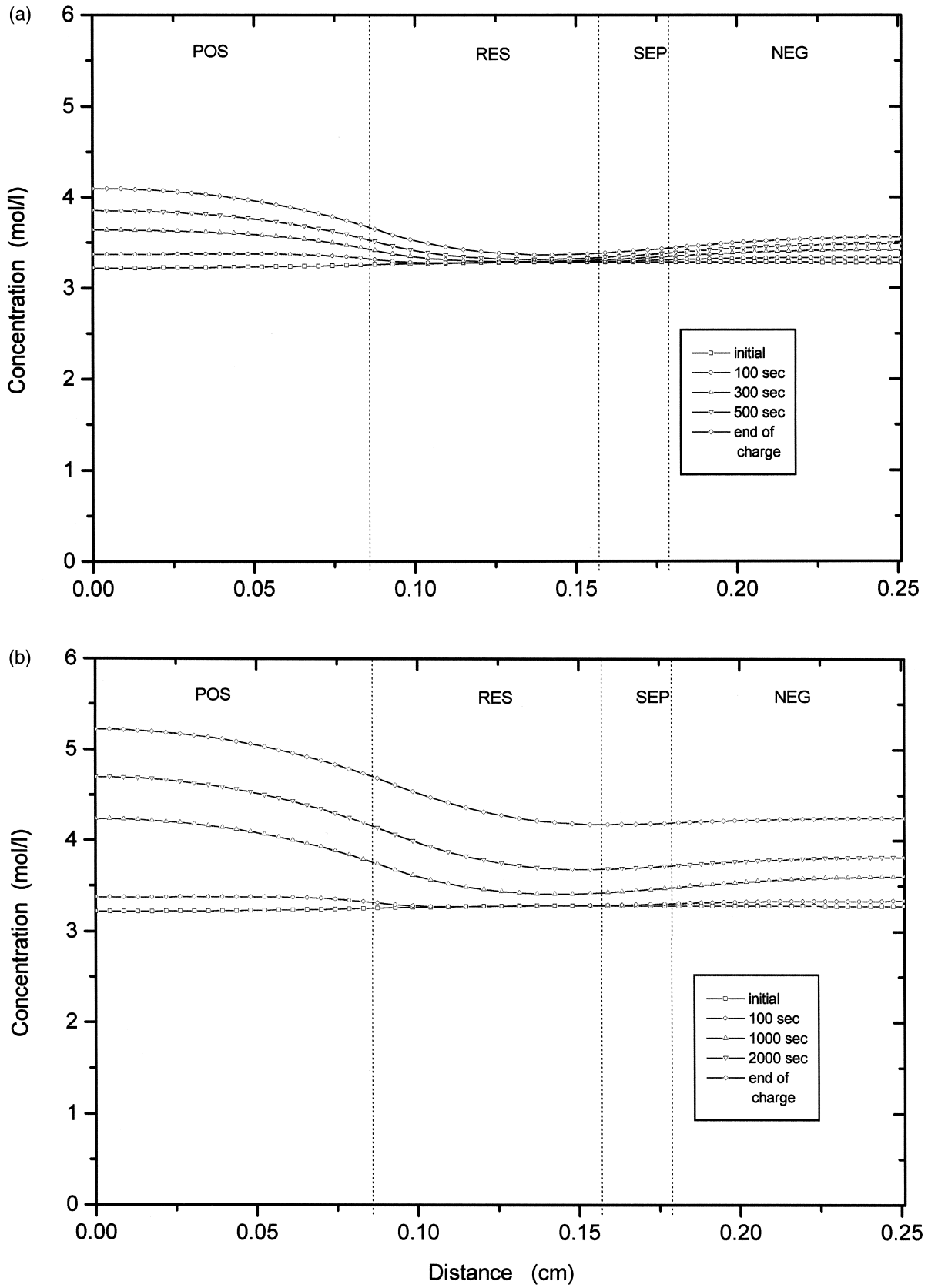

Fig. 4. Predicted profiles of acid concentration for 10 mA cm^{-2} charge at 25°C: (a) $j_{lim} = -1.0$ A cm^{-3}, (b) $j_{lim} = -5.0$ A cm^{-3}, (c) $j_{lim} = -10.0$ A cm^{-3}, (d) $j_{lim} = -$infinite.

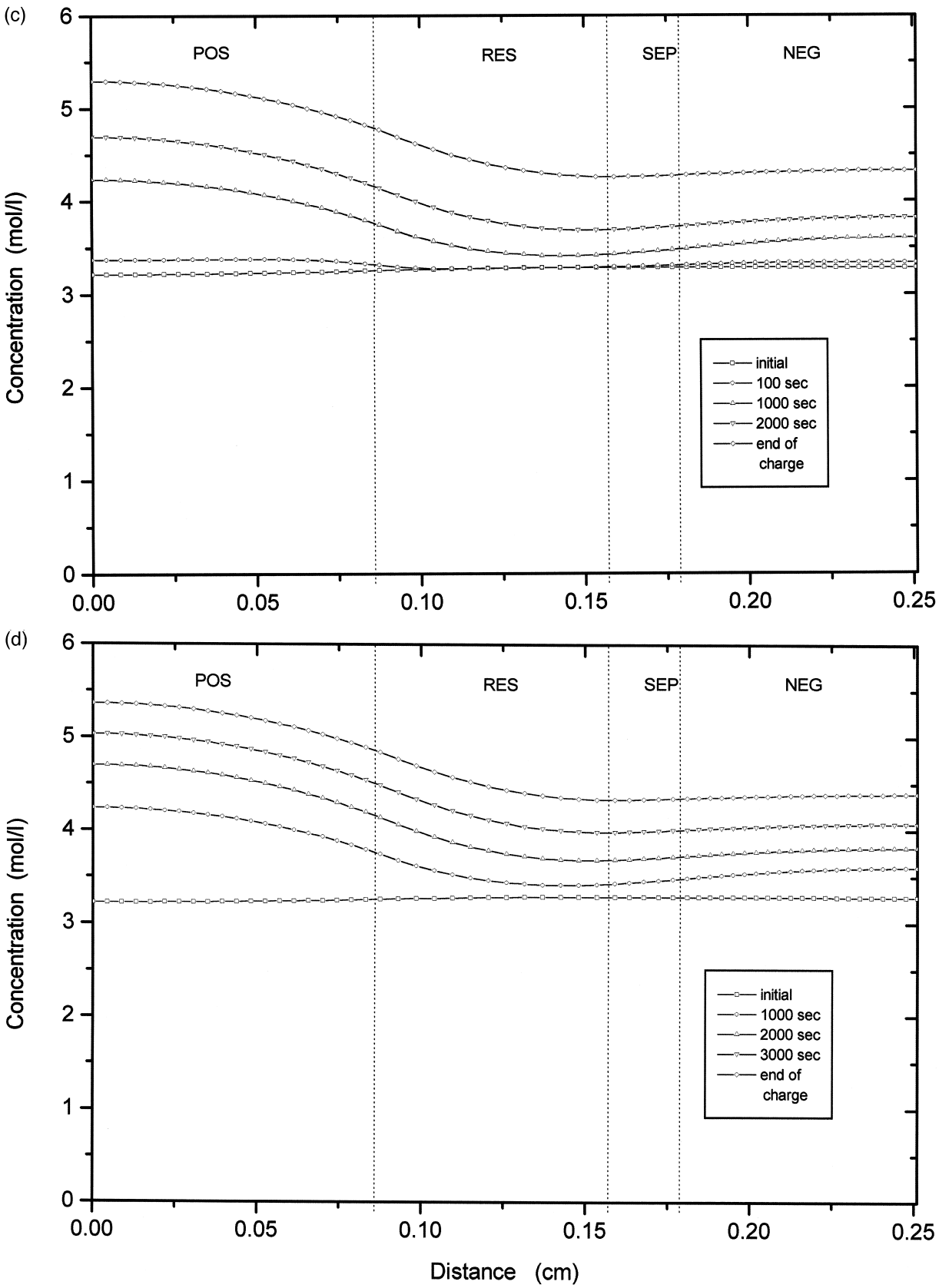

Fig. 4 (*continued*).

voltage cut-off are 47,762, 8295, 3255 and 424 s, respectively. As the charging current is increased, the internal resistance of the cell is higher due to the limitation of mass transfer of lead ions [16]. With time, therefore, high-rate charging shows a steeper rise in the cell voltage. This is because the internal resistance has a greater effect on the voltage penalty.

The concentration distribution in the cell is demonstrated with the same conditions as in Fig. 5. When the current density is 1 mA cm^{-2}, the distribution of electrolyte concentration with time is represented in Fig. 6(a). The charge returned is about 98% of the previous discharge. The concentration in the cell during charge was relatively uniform, which indicates the lower internal resistance of the cell. The limiting current density is -3.0 A cm^{-3} and the solid-state reaction, in this case, is not ignored as shown in Fig. 3. After the end of the charge process, the concentration difference between the end of the positive electrode and that of the negative electrode is very low; thus, the increment of the internal resistance due to the concentration gradient is not larger. When the charging current density is 5 mA cm^{-2}, about 85% of the discharge is restored, as shown in Fig. 6(b). As the charging current density increases, the time to the voltage cut-off is shortened but the concentration gradient is increased. In particular, the concentration gradient is maximum at the interface between the positive electrode and the reservoir. For a charging current density of 10 mA cm^{-2}, approximately 67% of the previous discharge is returned. The concentration distribution in the positive electrode shows that the gradient is much steeper than that in the other regions. As shown in Fig. 6(b), the concentration gradient is much higher at the interface between the positive electrode and the reservoir. Therefore, the resistance of the mass transfer in this region increases with increasing charging current density. On charging the battery at high rates, the charging efficiency is lower due to the concentration polarization and the voltage rise at the beginning of charge. At a charging current density of 20 mA cm^{-2}, the concentration profile in the cell has a nonuniform distribution, as demonstrated in Fig. 6(d). Note that the concentration near the current-collector of the positive electrode is markedly higher and there is a site at which the electrolyte concentration is largely unchanged in

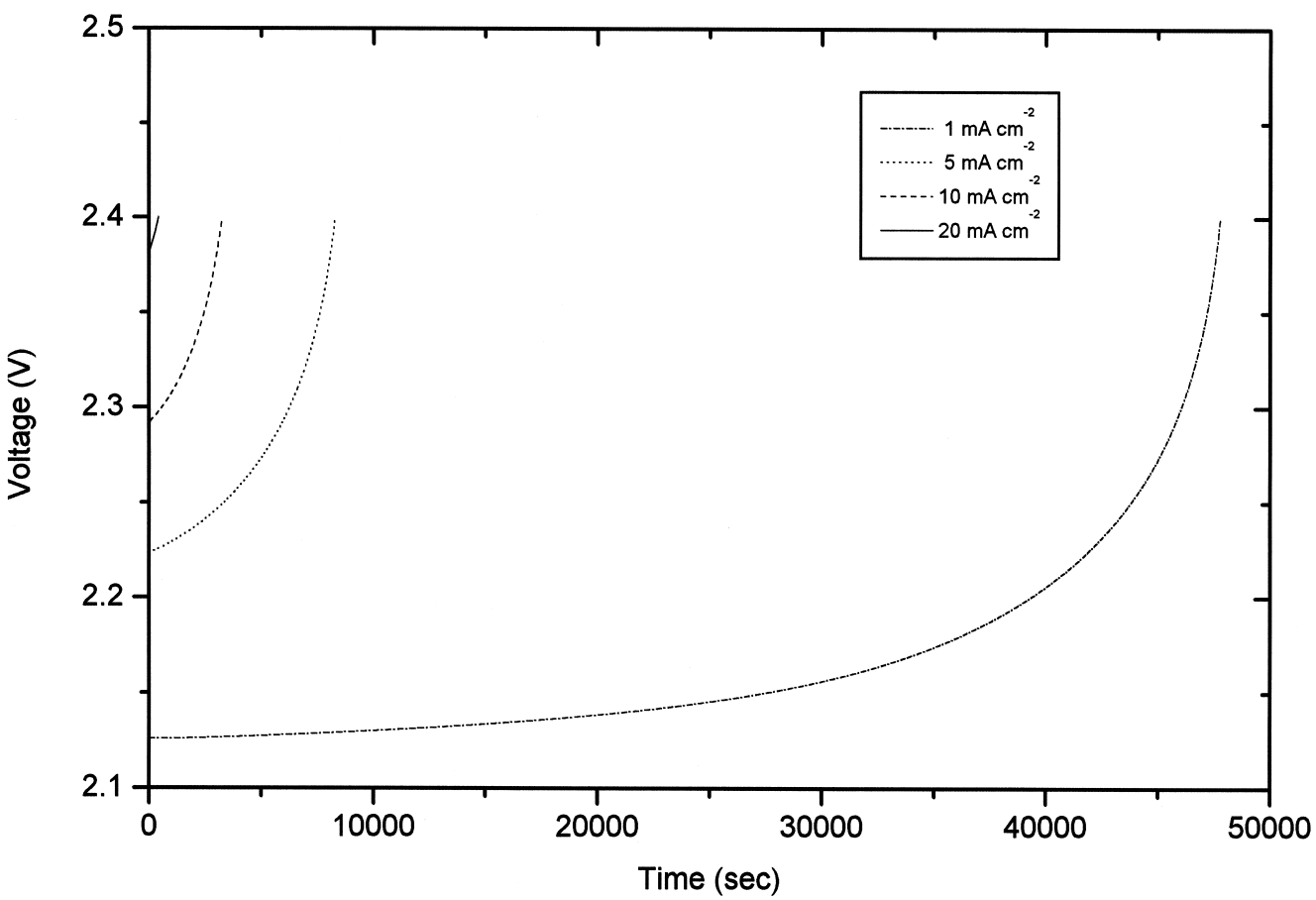

Fig. 5. Effect of charging current density for $j_{lim} = -3.0$ A cm^{-3} at 25°C.

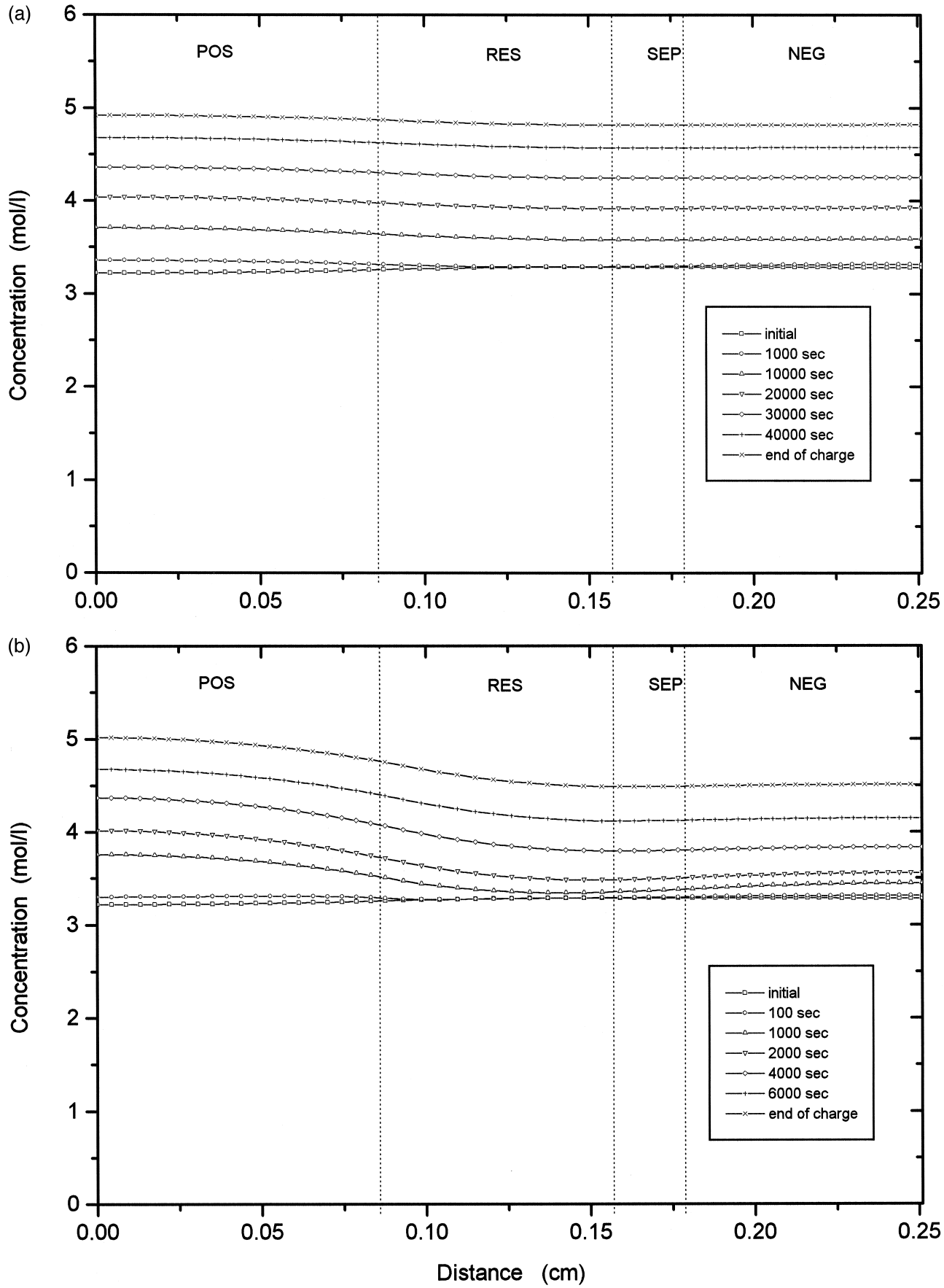

Fig. 6. Predicted profiles of acid concentration for $j_{\text{lim}} = -3.0$ A cm^{-3} at 25°C: (a) 1 mA cm^{-2}, (b) 5 mA cm^{-2}, (c) 10 mA cm^{-2}, (d) 20 mA cm^{-2}.

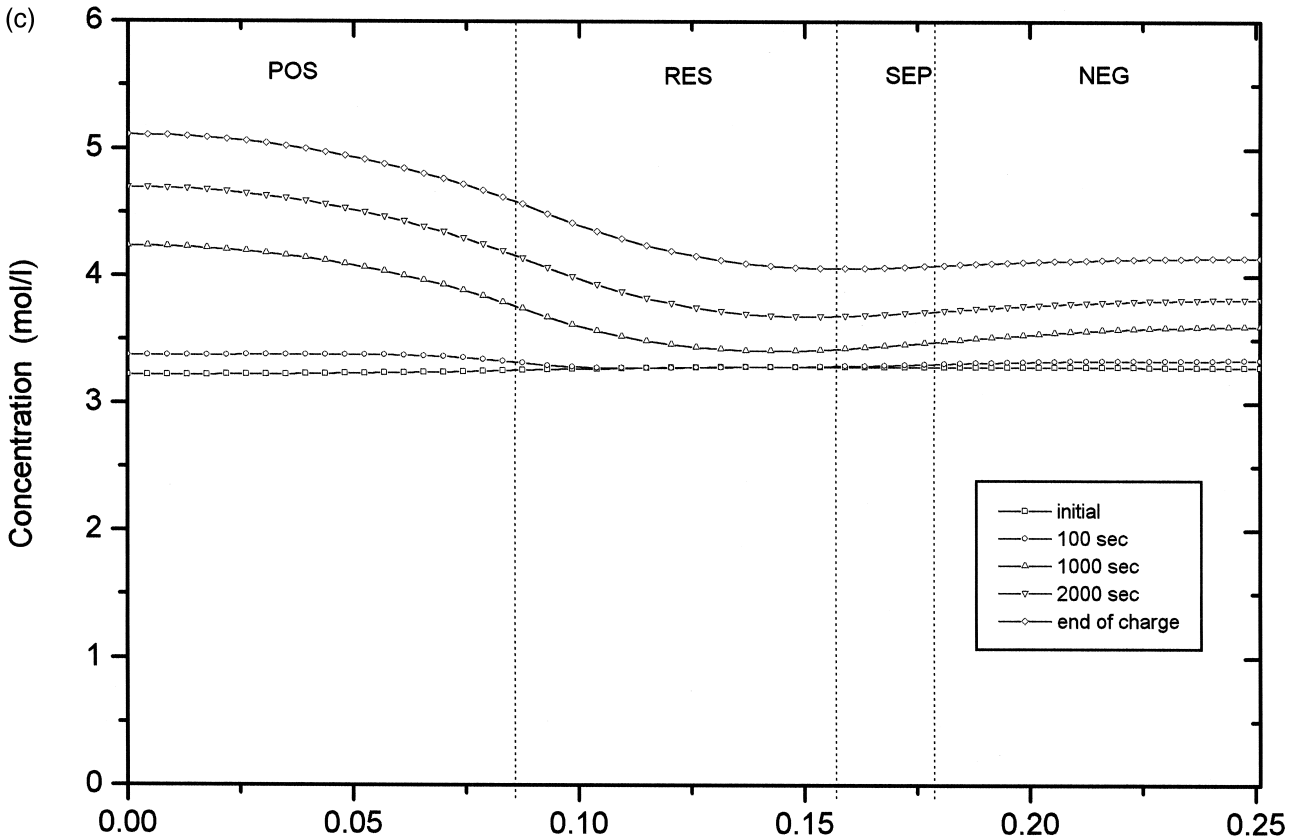

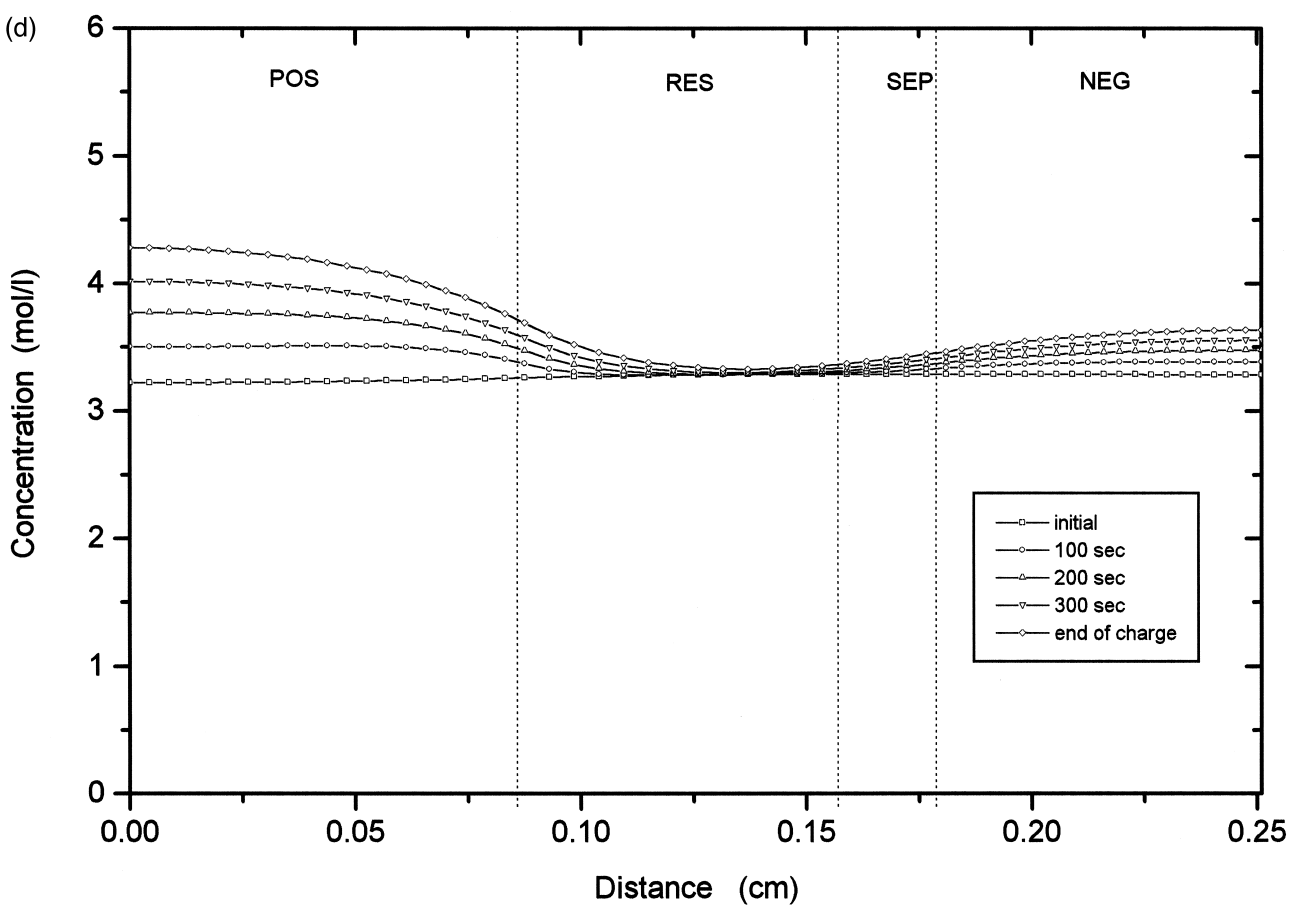

Fig. 6 (*continued*).

the reservoir. This is because the transfer resistance of charge produced both in the positive and negative electrode is higher.

4. Conclusions

The effect of various parameters on the cell performance for constant-current charge is investigated by means of a mathematical model. The results from applying the model can be summarized as follows.

(i) A higher value of the concentration exponent of charge reaction, γ, in the negative electrode has a greater effect on the charge performance than that in the positive electrode, due to increase in the voltage penalty.

(ii) The slope of the voltage rise at the initial state increases with increasing value of ζ, the morphology parameter. This means that the active surface area at the beginning of charge is low, and causes an increase in the internal resistance of the cell.

(iii) The charge at a low value of $-j_{\text{lim}}$ is inefficient because the charge performance is limited by the solid-state reaction rate in the negative electrode.

(iv) As the charging current density is increased, the concentration gradient has a maximum value at the interface between the positive electrode and the reservoir. Thus, the internal resistance of the cell becomes higher due to the limitation of the transfer rate of the electrolyte.

5. Symbols

a	active surface area of electrode ($cm^2\ cm^{-3}$)
a_1, a_2	coefficients used in governing equations and boundary conditions
$a_{\max}$	maximum specific active surface area of electrode ($cm^2\ cm^{-3}$)
c	concentration of binary electrolyte (mol cm^{-3})
c_{ref}	reference concentration of the binary electrolyte (mol cm^{-3})
D	diffusion coefficient of the binary electrolyte ($cm^2\ s^{-1}$)
F	Faraday's constant (96,487 C mol^{-1})
i	total applied current density based on projected electrode area (A cm^{-2})
i_1	current density in solid phase (A cm^{-2})
i_2	current density in conducting liquid phase (A cm^{-2})
$i_{\text{o1,ref}}$	exchange current density at c_{ref} for positive electrode (A cm^{-2})
$i_{\text{o4,ref}}$	exchange current density at c_{ref} for negative electrode (A cm^{-2})
j	reaction current per unit volume of electrode (A cm^{-3})
j_{lim}	limiting current density for negative electrode (A cm^{-3})
MW_i	molecular weight of species i (g mol^{-1})
Q	charge density in electrode (C cm^{-3})
$Q_{\max}$	theoretical maximum capacity (C cm^{-3})
R	universal gas constant (8.3143 J $mol^{-1}\ K^{-1}$)
t	time (s)
t_+^0	transference number of H^+ with respect to solvent velocity
T	absolute temperature (K)
U_{PbO_2}	equilibrium potential at c_{ref} for positive electrode (V)
v^*	volume − average velocity (cm s^{-1})
x	distance from centre of positive electrode (cm)

Greek letters

α_{a1}	anodic transfer coefficient for positive electrode
α_{c1}	cathodic transfer coefficient for positive electrode
α_{a4}	anodic transfer coefficient for negative electrode
α_{c4}	cathodic transfer coefficient for negative electrode
γ_1	concentration exponent for positive electrode
γ_4	concentration exponent for negative electrode
ε	porosity
ε_{sep}	porosity of separator
$\varepsilon_{\text{PbO}_{2,\text{ini}}}$	porosity of positive electrode at initial state-of-charge reaction
$\varepsilon_{\text{Pb,ini}}$	porosity of negative electrode at initial state-of-charge reaction
ζ_1	morphology parameter for positive electrode
ζ_4	morphology parameter for negative electrode
η	total local overpotential with respect to equilibrium potential
κ	electrolyte conductivity (S cm^{-1})
ρ_i	density of species i (g cm^{-3})
σ_i	conductivity of electrode matrix (S cm^{-1})
ϕ_1	potential in electrode matrix (V)
ϕ_2	potential in solution (V)

Superscripts

ex	exponent on porosity
exm	empirically determined constant for tortuosity of solid matrix

Acknowledgements

Grateful acknowledgement is made to Korea Storage Battery, Ltd. for support of this work.

References

[1] M. Maja, G. Morello, P. Spinelli, J. Power Sources 40 (1992) 81.
[2] E.M. Valeriote, D.M. Jochim, J. Power Sources 40 (1992) 93.
[3] T.G. Chang, E.M. Valeriote, D.M. Jochim, J. Power Sources 48 (1994) 163.
[4] H. Gu, T.V. Nguyen, R.E. White, J. Electrochem. Soc. 134 (1987) 2953.

[5] W.B. Gu, C.Y. Wang, B.Y. Liaw, J. Electrochem. Soc. 144 (1997) 2053.
[6] P. Ekdunge, K.V. Rybalka, D. Simonsson, Electrochim. Acta 32 (1987) 659.
[7] J. Newman, W. Tiedemann, AIChE J. 21 (1975) 25.
[8] S.C. Kim, W.H. Hong, J. Power Sources 77 (1999) 74.
[9] S.C. Kim, W.H. Hong, Hwahak Konghak 37 (1999) 336.
[10] P. De Vidts, R.E. White, J. Electrochem. Soc. 144 (1997) 1343.
[11] W.G. Sunu, in: R.E. White (Ed.), Electrochemical Cell Design, Plenum, New York, 1984, p. 357.
[12] H.A. Preisig, R.E. White, Comp. Chem. Eng. 14 (1990) 179.
[13] D. Fan, R.E. White, J. Electrochem. Soc. 138 (1991) 1688.
[14] T.V. Nguyen, Ph.D. Dissertation, Texas A&M Univ., College Station, TX, 1988.
[15] D.M. Bernardi, M.K. Carpenter, J. Electrochem. Soc. 142 (1995) 2631.
[16] J. Newman, W. Tiedemann, J. Electrochem. Soc. 144 (1997) 3081.